An Embedded System of the Measurement Instrument Applied in Aluminum Electrolytic Cells

Xin Ji[1], Zhaohui Zhang[1 2 †], Xiaoyan Zhao[1 2], Tianyao Zhang[1 2] and Yan Chen[1 2]

[1] School of Automation & Electrical Engineering, University of Science and Technology Beijing, 30# Xueyuan Road, Haidian District, Beijing 100083, China
m202220776@xs.ustb.edu.cn

[2] Beijing Engineering Research Center of Industrial Spectrum Imaging, 30# Xueyuan Road, Haidian District, Beijing 100083, China
zhangzhaohui@ustb.edu.cn

Abstract. The modern method for aluminum production is electrolysis, which extracts molten aluminum from a mixture of cryolite and alumina. During the aluminum electrolysis process, due to density differences, the molten aluminum settles at the bottom while the electrolyte remains on top. The balance of the heights of the molten aluminum and the electrolyte directly affects the current efficiency during aluminum production. Given the enormous current involved in the electrolysis process, even a slight reduction in current efficiency can lead to significant energy wastage. Therefore, maintaining the balance between the molten aluminum and the electrolyte requires regular measurements to adjust feeding strategies. However, the current measurement method is manual, time-consuming, labor-intensive, and cannot provide real-time height data. This paper addresses the issue of strong interference in the measurement of key parameters in aluminum electrolysis production and presents the design and implementation of an embedded electronic system based on an ARM processor. The system is designed to interface with sensors and various peripheral devices. Through manual and automatic control, multiple parameters within the electrolytic cell could be measured and displayed in real time. Field test results indicated that this system effectively obtained precise data on the aluminum electrolysis production process, potentially becoming a fundamental component for the intelligentization of aluminum production in the future.

Keywords: Electrolytic aluminum, Measurement Instrument, Embedded system, Real-time operating system.

1 Introduction

Electrolytic aluminum is an important lightweight metal with extensive applications. However, the production of electrolytic aluminum is a highly energy-intensive process, requiring substantial electricity per ton of molten aluminum. The continuous consumption of electrolytes leads to a decrease in current efficiency. The primary aluminum industry, as a typical energy-intensive sector, emits more greenhouse gases

than other non-ferrous metal industries, accounting for more than 3% of global emissions. As the world's largest producer and consumer of primary aluminum (accounting for 57% of global production), China bears significant responsibility for energy conservation and emission reduction. Therefore, China has proposed a dual carbon strategy to guide the electrolytic aluminum industry towards high-end, intelligent, and green development. The aluminum electrolytic cell, operating at 500,000 amperes and 950 degrees Celsius, is the core equipment for producing high-quality aluminum. Its condition directly affects energy consumption, raw material consumption, and product quality [1-3]. By using comprehensive measurement instruments for aluminum electrolytic cells, it is possible to monitor the heights and temperatures of the electrolyte and molten aluminum in real-time during production. This ensures timely addition of raw materials, adjustment of electrode spacing, and control of aluminum output time and tonnage, thereby reducing energy consumption and carbon emissions per ton of aluminum.

Currently, domestic measurement of the two levels in aluminum electrolytic cells relies on manual methods, using F rods to observe color changes of adhesions. Foreign products, such as the ProH Laser Sensor by Sweden's Precimeter and the non-contact disc sensor by the US's Rayteq, provide stable readings even under steam or smoke interference. Domestically, Shi Yanfei’s team [4] developed an inspection robot for online measurement of the two levels, while Researcher Zeng Shuiping [5] from North China University of Technology developed a device with 8-12 temperature nodes inserted into the electrolytic cell to infer aluminum levels from temperature changes. Wang Junqing [6] designed a multi-parameter detection system for aluminum electrolytic cells, and Aroba [7] and colleagues used electromagnetic induction to determine molten metal levels but could not measure the aluminum under the electrolyte in real-time. These methods fail to meet the requirements for online and automated measurement.

We have developed an embedded comprehensive measurement device for aluminum electrolytic cells, achieving automated measurement and result display without opening the furnace door, thus reducing safety hazards. The embedded system is designed to integrate seamlessly with existing production processes, providing accurate and reliable real-time data on key parameters such as the heights of molten aluminum and electrolyte, and their respective temperatures. This device not only enhances the safety and efficiency of the measurement process but also supports the broader goals of intelligent and green development in the electrolytic aluminum industry by enabling more precise control and optimization of production parameters.The embedded system offers scalability and customization, which is particularly advantageous in the complex multi-physical field coupling environment of aluminum electrolysis. On the hardware side, sensors, processors, and power modules can be tailored, with a fixed number of interfaces designed to minimize external signal interference. On the software side, the operating system, control algorithms, and communication protocols can be streamlined by removing unnecessary functionalities, thereby enhancing system response speed and stability. Thus, the precise control and efficient operation throughout the production process have been enabled.

2 Hardware Design

2.1 Overall Design

This system is designed to address the complex environment within aluminum electrolytic cells, where multiple physical fields are coupled. It can automatically measure the heights of electrolyte and molten aluminum, as well as the internal temperature of the cell. Firstly, the embedded electronic system must be equipped with a variety of sensor interfaces, enabling it to process commands and facilitate data communication. Secondly, it is required to operate with long-term stability in environments with strong electromagnetic interference. Thirdly, the system should incorporate a visualization module to provide real-time display of measurement results.

The overall hardware connection framework of the system is shown in Figure 1. The system's overall structure comprises multiple input and control signals, including limit, position, control, liquid level, temperature signals, proximity switches, encoders, external buttons, probe sensors, and an RS485 converter. These signals are first passed through a voltage conversion circuit and processed by the STM32F407 and its peripheral circuits. The STM32F407 then outputs control signals to actuators, computers, and an LED display, enabling mechanical actions, data exchange with the upper computer, and display of system status or measurements. The system utilizes various sensors and communication modules to monitor environmental and equipment conditions, while control signals operate external devices. The modular design of the embedded hardware enables customization of interface connections, reducing the potential for electromagnetic interference.

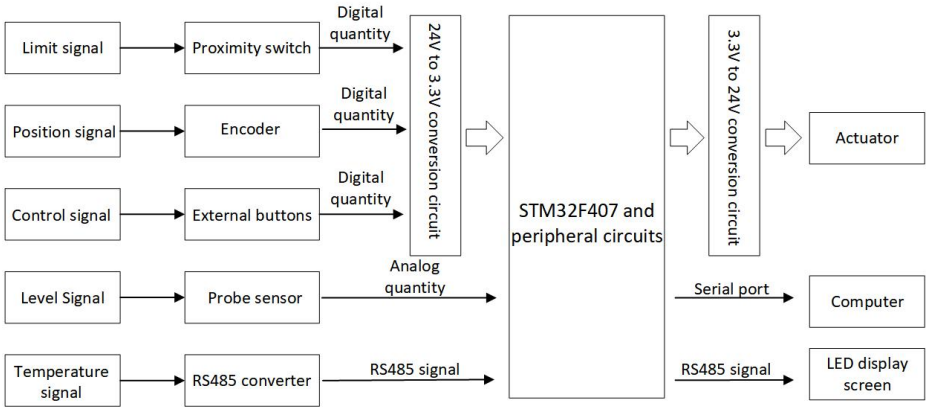

Fig. 1. Overall system hardware design framework .

2.2 Embedded Electronic System

As the core of the system, the embedded electronic system performs several critical functions, including ADC interfaces, encoder pulse capture, 24V actuator control and

feedback, RS485 communication, and multitasking capabilities for real-time control of displacement feedback and motion. Specific parameters are detailed in Table 1. We selected the STM32F407ZGT6 MCU, based on the ARM core, and designed the peripheral circuits, including power interfaces, digital and analog input/output ports, drivers for various peripheral interfaces, and communication interfaces.

Table 1. Embedded system interface parameters.

Interface	Signal type	Voltage
Proximity switch	Digital input	12~24V DC
Encoder	Digital input	0~5V DC
External buttons	Digital input	24V DC
Probe sensor	Analog input	0~5V DC
RS485 converter	Analog input/output	±5V DC
Electric relay	Digital output	12~24V DC
Solenoid valve	Digital output	24V DC
Serial port	Digital output	3.3V DC

The designed PCB for the embedded electronic system is shown in Figure 2. Firstly, the design dimensions are critical. An excessively large size results in longer printed circuits, which increases impedance, reduces noise resistance, and raises costs. Conversely, an overly small size can lead to inadequate heat dissipation and heightened susceptibility to interference between adjacent traces. Considering the reserved dimensions and installation requirements for mounting within an electrical cabinet, the embedded electronic system is designed with dimensions of 100mm × 100mm. To minimize interference, we strategically arranged the power lines, isolating the 24V power supply from other power sources. To further prevent power system interference, DC/DC power isolation modules were utilized to avoid mutual interference between power modules. Additionally, we designed filter circuits by placing capacitors between the positive and negative power supply terminals of each power chip, effectively filtering out high-frequency noise at the power pins and reducing the impact of power impurities on the circuit.

In the layout process, we considered the ease of signal flow, maintaining the consistency of signal flow direction as much as possible, and arranging components uniformly and neatly on the PCB to shorten the trace lengths. Components close to the chip in the schematic were placed near the chip's package during layout [9]. To reduce interference and prevent power lines from forming loops, ground lines were thickened, and signal lines on different layers were routed perpendicularly to each other. After verifying the design, we labeled each component on the PCB and set up some test points for debugging, such as 3.3V, 5V, and GND. Considering the high dust environment in the electrolytic aluminium production workshop, it is necessary

to cover the components on the final debugged board with a dust cover, so the component parts are distributed in the middle position of the board, with mounting holes reserved at the corners.

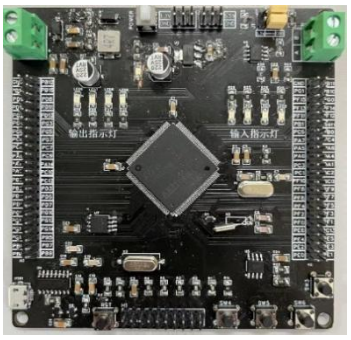

Fig. 2. Embedded Electronic Systems PCB.

2.3 Drivinge Board Design

Considering the strong magnetic environment on-site, electromagnetic compatibility (EMC) issues must be addressed. An optocoupler isolation circuit has been adopted to convert high-voltage, noise-laden signals into low-voltage, safe signals, ensuring signal compatibility between different devices. Additionally, this circuit provides electrical isolation, effectively shielding the control system from electromagnetic interference in the aluminum electrolysis environment and ensuring stable signal transmission. The optocoupler also prevents high-voltage backflow in case of equipment failure, protecting sensitive components such as microcontrollers, and enhancing the reliability and stability of the embedded system. At the same time, the power supply must account for the limitations of the STM32 series chips, where most pins can tolerate up to 3.3V, with only a few capable of handling 5V. However, the sensors used in the system, such as relays and solenoid valves, operate at 24V. Therefore, the controller needs the ability to drive 24V actuators, and when capturing encoder pulses, the pins must also be capable of receiving 24V signals. The implementation of this circuit effectively addresses these challenges. We referenced an optocoupler isolation circuit solution. The standard for choosing an optocoupler isolation circuit [10] typically requires its switching frequency to be at least ten times higher than the required frequency. The frequency of the encoder pulses can be calculated as follows:

$$f = \frac{X \diagup P}{T} \tag{1}$$

The resolution f of the encoder output is equal to 0.001953125mm/pulse. The measured travel distance X is 1200mm, with a measurement time ranging from 10 to 25 seconds, with a maximum of 61440 pulses. The optocoupler's switching speed

needs to exceed ten times the frequency. The $EL817$ optocoupler is selected, with a switching speed of $1MHZ$. The 24V to 3.3V simulation circuit is shown in Figure 3.

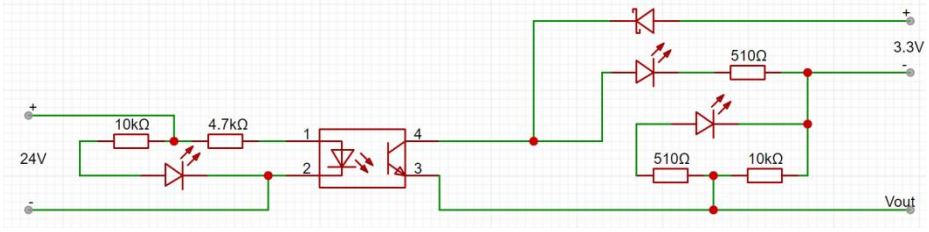

Fig. 3. 24V-3.3V conversion circuit.

To drive 24V actuators, a 3.3V to 24V voltage conversion circuit is required, as illustrated in Figure 4. An optocoupler isolation circuit uses MOSFETs for driving. The electromagnetic valve starts in a grounded state, and a P-channel MOSFET acts as a high-side switch connected to 24V. The gate controls the switch, with the source at the high level and the drain at the output. The IRFR5305 chip is selected for its voltage resistance and thermal dissipation capabilities. The control signal from the STM32, after passing through the optocoupler, connects to the 24V input via the MOSFET. Pin 1 serves as the gate control, pin 3 as the source; when the voltages at pins 1 and 3 exceed the turn-on voltage, the drain activates the electromagnetic valve.

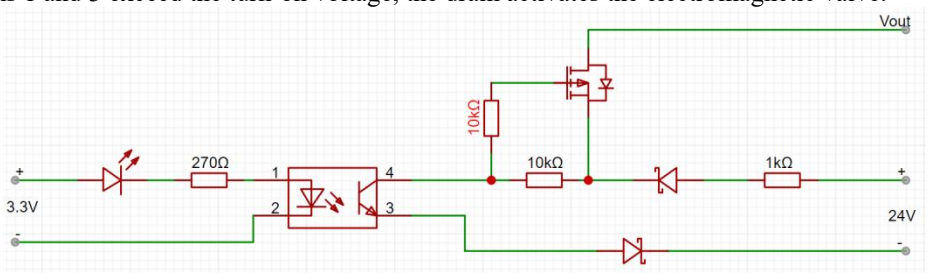

Fig. 4. 3.3V-24V conversion circuit.

The sensor signal is in the range of 0-10V, while the maximum voltage of the STM32 series chip is 3.3V. Hence, voltage matching design is necessary for the ADC acquisition circuit. The data acquisition circuit primarily consists of a pre-divider circuit and a voltage follower. The pre-divider circuit comprises divider resistors, with U0 representing the voltage obtained from the divider, as illustrated by design formula (2).

$$U_O = \frac{R_1}{R_1 + R_2} \times U_{probe} \tag{2}$$

In the actual hardware circuit design, $1K\Omega$ and $2K\Omega$ resistors are selected as R_1 and R_2 to reduce the voltage to one-third of the original, so that the ADC input voltage is within the normal range of the control chip. The voltage follower is

configured as a common-collector circuit, with the voltage signal input at the base and output at the emitter. This configuration is characterized by high input impedance and low output impedance, drawing minimal current from the signal source, and possessing strong load-driving capability. The input voltage and output voltage are in phase, with a voltage gain approximately equal to 1. The simulation of the ADC acquisition circuit is shown in Figure 5.

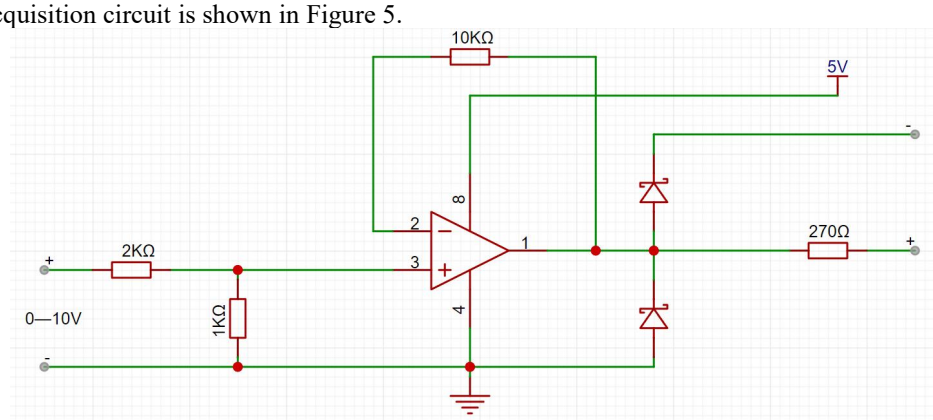

Fig. 5. ADC acquisition circuit.

3 Software Design

3.1 Software Hierarchy Design

Based on the actual measurement requirements, the system needs to maintain stable operation in a strong magnetic environment while supporting multitasking capabilities. Therefore, we selected the µC/OS-III embedded operating system [12] and ported it to the STM32F407, writing the necessary drivers for the hardware modules and sensors. µC/OS-III is a soft real-time operating system, where tasks are typically able to respond in a timely manner, and occasional delays do not lead to critical issues. Key tasks such as data collection, motor control, and cylinder movement were assigned higher priority levels to ensure they received sufficient CPU resources for prompt responses to external events. By developing efficient interrupt service routines, the system is able to promptly respond to external signals or hardware interrupts. Additionally, the system's time-slicing scheduling function ensures that all tasks are executed within the required time frame, thus ensuring the system's overall real-time performance and reliability.The controller performs real-time sensor readings, feedback control of mechanical movements, and communication functions, enabling various tasks to work collaboratively. The software design hierarchy is shown in the Figure 6.

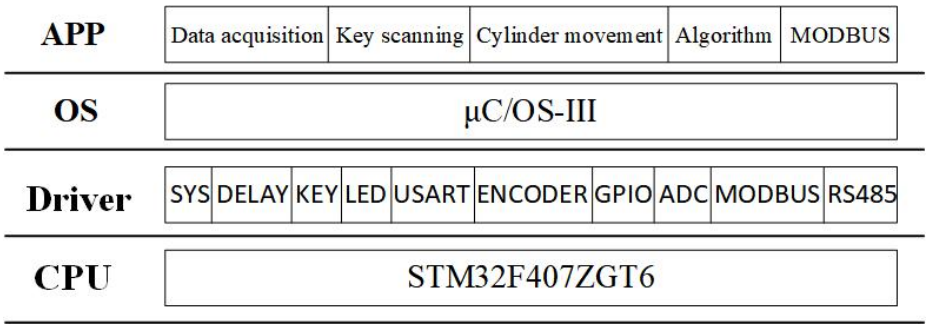

Fig. 6. Software design hierarchy.

This system architecture consists of four layers: the CPU Layer, Driver Layer, OS Layer, and APP Layer. The CPU Layer interfaces with the CPU using KEIL platform's MDK5 firmware library functions and configures components like RAM and FLASH. The Driver Layer provides encapsulated driver functions for various hardware modules and sensors, such as ENCODER interfaces, GPIO, ADC, clock, interrupts, buttons, LEDs, USART, RS485, and MODBUS. The OS Layer employs the μC/OS-III embedded operating system for task scheduling and synchronization, which simplifies software design by managing task concurrency and enhancing development efficiency and system stability. Finally, the APP Layer, operating on top of the OS Layer, implements upper-level functions such as data acquisition, button scanning, cylinder movement, algorithm processing, and MODBUS communication by invoking lower-level functions.

3.2 Programming and Implementation

Upon powering up the device, the system initializes the main controller chip's clock, interrupts, and other essential configurations. Once the system initialization is complete, it proceeds with initializing the peripheral modules and sensors, including the LED, KEY, ENCODER, GPIO, ADC, RS485, and MODBUS interfaces. Following this, the μC/OS-III operating system is initialized, involving the setup of task management and the creation of idle tasks, clock tasks, and statistical task timing modules.

After the initial setup, μC/OS-III awaits the creation of user-defined tasks. To achieve this, a "Start" task is created to initialize other driver-based user tasks, such as data acquisition, key scanning, cylinder movement, algorithm processing, stop limit monitoring, and MODBUS communication tasks. The "Start" task is solely responsible for creating these user tasks [13]. The program then operates according to the flowchart shown below.

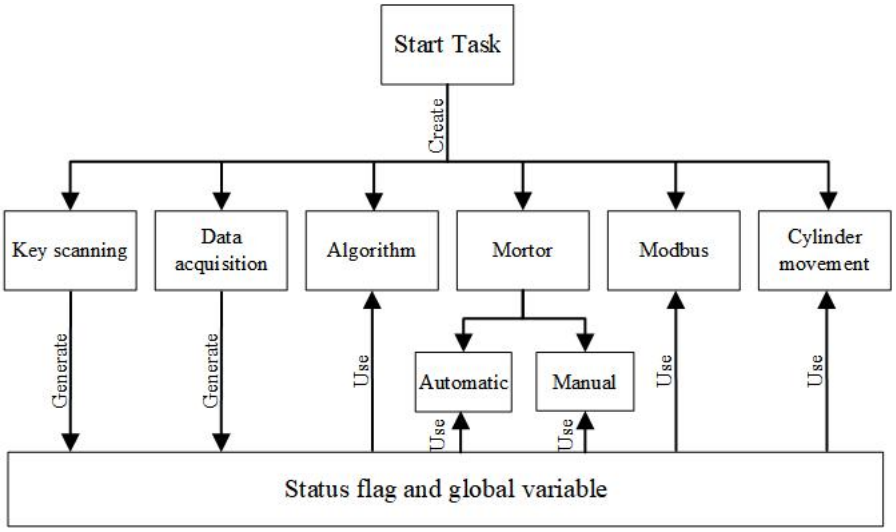

Fig. 7. Program flow chart.

4 Experiments

In the analysis of the position-impedance waveform, as shown in Figure 8, we first applied cubic spline interpolation to smoothly fit the nonlinear portions of the data. Then, based on a cumulative difference algorithm, we identified the boundary points between air-electrolyte and electrolyte-aluminum. The difference formula is as follows:

$$\mathrm{d(i)} = z(i+1) - z(i) \tag{3}$$

The boundary between the electrolyte and air is relatively easy to identify, as it can be determined by checking if the difference value exceeds a certain threshold. However, identifying the boundary between the electrolyte and aluminum is more challenging due to the uneven distribution of the concentration field in the electrolytic cell, where electrochemical reactions occur continuously to varying degrees. Additionally, the precision of the probe's voltage detection is limited, causing the voltage values to fluctuate sharply within a small range, making it difficult to discern the exact boundary. To address this, we propose an evaluation criterion to select potential boundary points by calculating the ratio of the slopes before and after each point, denoted as K. The point where K reaches its maximum is identified as the desired boundary point.

$$K = \frac{S_1}{S_2} \tag{4}$$

In the equation, S_1 represents the slope over a fixed interval before the point, and S_2 represents the slope over a fixed interval after the point, with K as the evaluation criterion. The results are then labeled on Figure 8. At the initiation of the measurement, the sensor is positioned in air, exhibiting infinite impedance.

Subsequently, as the sensor immerses into the molten electrolyte, corresponding to point A in the graph, the impedance gradually decreases. As the sensor further descends into the molten aluminum, the impedance experiences a subsequent decline [14]. Conversely, during the ascent of the sensor, the impedance variation curve exhibits an inverse trend.

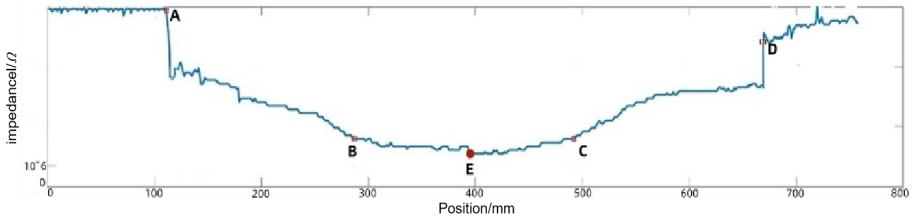

Fig. 8. Impedance Distribution Along Sensor Position.

Through multiple measurements and subsequent analysis, the data obtained from this embedded electronic system were compared with manually collected data, as depicted in Table 2. The electrolyte height measured by the device yielded an average value of 154.83 mm, with a standard deviation of 3.43 mm, indicating some variability. In contrast, manual measurements were conducted by inserting an F-rod into the electrolytic cell and withdrawing it after a short time, followed by observing the color change of the adhering material. This method introduced a degree of human error, resulting in a measurement of 160 ± 5 mm with a standard deviation of 5 mm. In summary, the embedded device demonstrated better data stability compared to manual measurements when performing multiple measurements in a short period.

Table 2. Comparison between Instrument and Manual Measurements.

Numbers	Instrument measurement	Manual measurement
1	152	160±5
2	161	160±5
3	156	160±5
4	153	160±5
5	152	160±5
6	155	160±5

5 Conclusion

This article custom-developed an embedded electronic system based on the μC/OS-III real-time operating system, utilizing ARM processors. Specific chips were selected according to the actual needs of the device, and voltage conversion circuits were designed to ensure the ability to drive high voltages. Additionally, acquisition circuits were designed to ensure stable voltage input. Software development was carried out based on the overall requirements of the device logic, after porting the μC/OS-III real-time operating system. Through laboratory testing, it was demonstrated that the system could achieve real-time communication for multiple tasks and accomplish the measurement of key parameters within the aluminum electrolytic cell.

References

1. Tabereaux A T, Peterson R D. Aluminum production[M]//Treatise on process metallurgy. Elsevier, 2024: 625-676.
2. Shen A, Zhang J. Technologies for CO2 emission reduction and low-carbon development in primary aluminum industry in China: A review[J]. Renewable and Sustainable Energy Reviews, 2024, 189: 113965.
3. Hou W, Li H, Mao L I, et al. Effects of electrolysis process parameters on alumina dissolution and their optimization[J]. Transactions of Nonferrous Metals Society of China, 2020, 30(12): 3390-3403.
4. Shi Yanfei, Wu Zuhuai, Lu Hui. Development of Aluminum Electrolysis Inspection Robot Technology and Equipment[J]. Nonferrous Metal Design, 2023, 50(02):26-29. (in Chinese)
5. Zeng Shuiping, Zhang Qiuping, Zhang Yuhui, et al. A Method for Measuring Temperature and Aluminum Level in Aluminum Electrolysis Process [P]. Beijing: CN103954320B, 2016-05-18. (in Chinese)
6. Wang Junqing. Multi-parameter Detection System for Aluminum Electrolysis Cell [D]. North China University of Technology, 2005. (in Chinese)
7. Aroba Saleem, Peter Ross Underhill, David Chataway, Terry Gerritsen, Afshin Sadri, and Thomas W. Krause. Electromagnetic Measurement of Molten Metal Level in Pyrometallurgical Furnaces[J]. IEEE Transactions on Instrumentation and Measurement, 2020, 69(6): 3118-3125.
8. Zhang Zhaohui, Zhao Xiaoyan, Bian Xinxiao, et al. Impedance Measurement Method for Aluminum Electrolysis under Strong Magnetic Field Interference[J]. Metallurgical Automation, 2019, 43(04): 69-72. (in Chinese)
9. Lienig J, Scheible J. Fundamentals of layout design for electronic circuits[J]. 2020.
10. Altuğ B A, Kababiyik A, Dincol E, et al. Buck Converter with Optocoupler Based Switching[C]//2021 8th International Conference on Electrical and Electronics Engineering (ICEEE). IEEE, 2021: 184-190.
11. Prado E O, Bolsi P C, Sartori H C, et al. An overview about Si, Superjunction, SiC and GaN power MOSFET technologies in power electronics applications[J]. Energies, 2022, 15(14): 5244.
12. Jiang S Q, Zhu Z Y. Ship insulation monitoring and fault location system based on STM32[C]//2020 IEEE 18th International Conference on Industrial Informatics (INDIN). IEEE, 2020, 1: 851-856.

13. Kopetz H, Steiner W. Real-time systems: design principles for distributed embedded applications[M]. Springer Nature, 2022.
14. Wang, X., Peterson, R.D., Tabereaux, A.T. (2016). Electrical Conductivity of Cryolitic Melts, Essential Readings in Light Metals, Springer, Cham, 2016, pp. 57-64.